

Structural characterization and mechanisms of macrophage immunomodulatory activity of a pectic polysaccharide from *Cucurbita moschata* Duch.

Linlin Huang^{a,b}, Jing Zhao^{a,b}, Yunlu Wei^{a,b}, Guoyong Yu^{a,b}, Fei Li^{a,b}, Quanhong Li^{a,b,*}

^a College of Food Science and Nutritional Engineering, China Agricultural University, Beijing 100083, China

^b National Engineering Research Center for Fruits and Vegetables Processing, Beijing 100083, China

ARTICLE INFO

Keywords:

Pectic polysaccharide
Immunomodulatory activity
Structure
Macrophages

ABSTRACT

A pectic polysaccharide (named CMDP-4b) with a molecular weight of 31.97 kDa was extracted from *Cucurbita moschata* Duch and purified by column chromatography. On the basis of methylation, Fourier-transform infrared, monosaccharide composition, and one- and two-dimensional nuclear magnetic resonance spectroscopy analyses, the structure of CMDP-4b was determined to be composed of an α -1,4-linked homogalacturonan backbone, which was slightly acetylated and highly methyl-esterified, and branched at the O-3 position of the \rightarrow 4)- α -D-GalpA-6-OMe-(1 \rightarrow . Immunomodulatory assays showed that CMDP-4b not only induced the secretion of nitrous oxide and cytokines (i.e. IL-1 β , TNF- α , and IL-6) but also promoted pinocytic and phagocytic activities of macrophages, suggesting that CMDP-4b possessed immunomodulatory activity. Moreover, toll-like receptor 4 and complement receptor 3 may play a critical role in CMDP-4b-induced macrophage activation through the NF- κ B and the MAPKs signaling pathways. Our study provides the molecular basis for the potential use of CMDP-4b as a natural immunostimulant.

1. Introduction

Regulation of the immune responses is of critical importance in the prevention and treatments of multiple diseases. Macrophages are the main component in adaptive and innate immunity, and serve as the front-line defense against pathogens (Martinez et al., 2009). At present, plant-based polysaccharides have attracted considerable attention owing to their non-toxic nature and immunomodulatory activity, such as the regulatory effect on macrophages (Schepetkin & Quinn, 2006). These polysaccharides have been shown to bind to pattern recognition receptors on macrophages, such as complement receptor 3 (CR3), mannose receptors (MR), and toll-like receptors (TLRs), which can activate macrophages through different signaling pathways. Subsequently, activated macrophages kill pathogens through phagocytosis and, at the same time, release cytokines, chemokines, and nitrogen intermediates to trigger immune responses (Kanmani et al., 2018).

Pumpkin (*Cucurbita moschata* Duch.) is an herbaceous annual plant, a species of the family Cucurbitaceae, that is grown and consumed worldwide (Maran et al., 2013). *Cucurbita moschata* Duch. possesses

various biological activities, including anti-carcinogenic, antioxidant, anti-diabetic, anti-inflammatory, and immunomodulatory activities (Yadav et al., 2010). Pumpkin polysaccharide is the most famous bioactive component isolated from the pumpkin with high biological safety and excellent pharmacological effects (Chen & Huang, 2019). The biological activities of plant polysaccharides due to the special characteristics including their molecular weight, specific glycosidic linkages, monosaccharide composition, degree of branching, polymerization, and the spatial configuration of the chains (Mutallifu et al., 2020). Pectic polysaccharides constitute the main components of pumpkin polysaccharides and have multiple pharmacological activities (Minzanova et al., 2018). Immunomodulation is one of the most significant potential activities of pectic polysaccharides. The authors of a previous study reported that pectic polysaccharides had stronger immunomodulatory properties than neutral polysaccharides extracted from *Polygonum multiflorum* owing to the effects of molecular weight, branching, and the presence of uronic acid groups (Zhang et al., 2018). Patra et al. (2013) demonstrated that a pectic polysaccharides obtained from *Allium cepa* with a main chain comprising α -1,4-D-galacturonan had a significant

* Corresponding author at: College of Food Science and Nutritional Engineering, China Agricultural University, Qinghuadong Road No. 17, Haidian District, Beijing 100083, China.

E-mail address: quanhong_li@hotmail.com (Q. Li).

<https://doi.org/10.1016/j.carbpol.2021.118288>

Received 10 February 2021; Received in revised form 22 May 2021; Accepted 30 May 2021

Available online 2 June 2021

0144-8617/© 2021 Elsevier Ltd. All rights reserved.

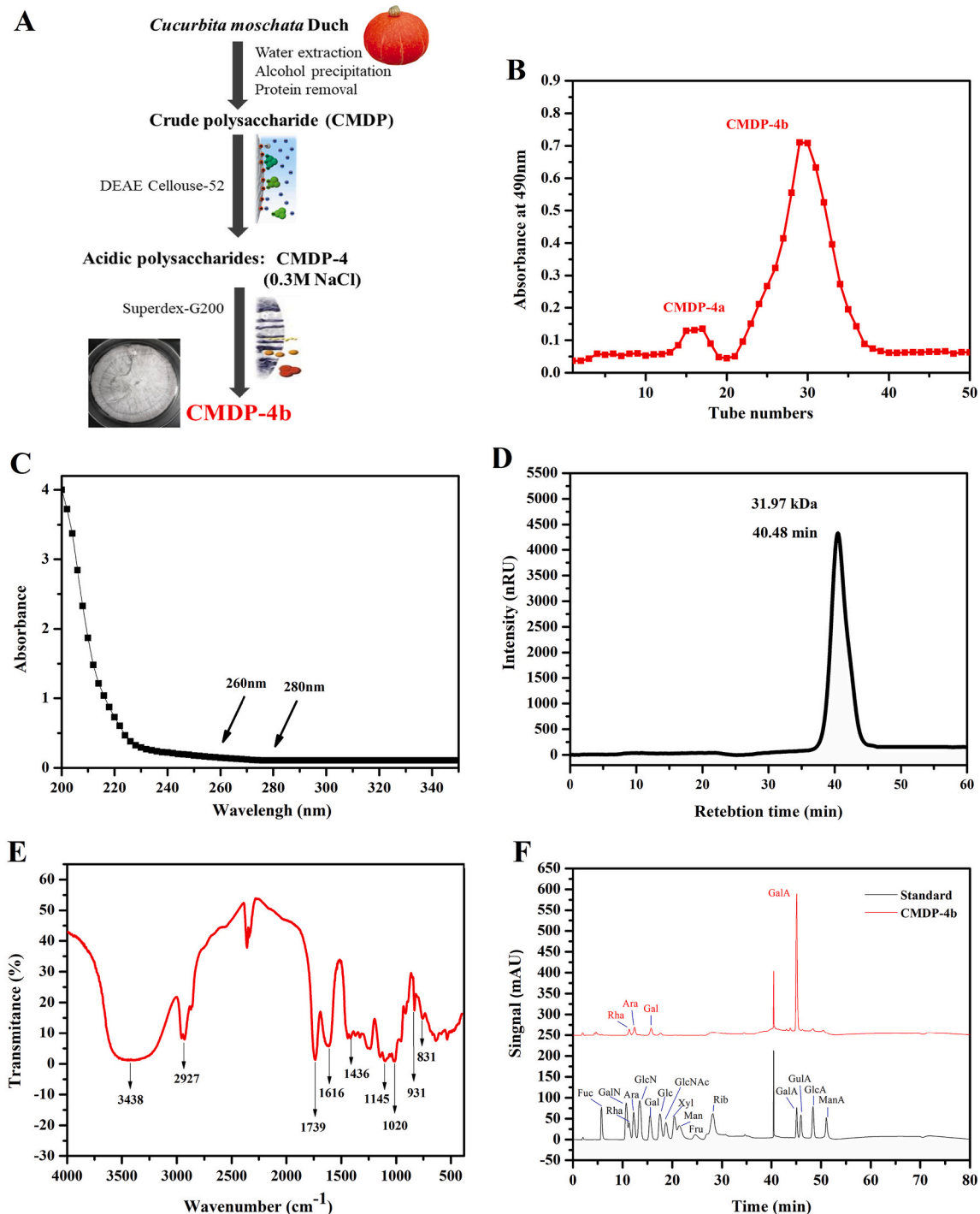


Fig. 1. (A) Procedure of CMDP-4b extraction and purification, (B) Elution profile of CMDP-4b from a Superdex-G200 column, (C) UV-visible spectrum of CMDP-4b, (D) HPGPC of CMDP-4b, (E) FT-IR spectrum of CMDP-4b; (F) HPIEC of monosaccharide standards and CMDP-4b.

effect on the activation of splenocytes, thymocytes, and macrophages. Our recent studies have shown that pumpkin pectic polysaccharides protect pancreatic β -cells from oxidative damage (Li et al., 2021) and alleviate type 2 diabetes in rats by regulating the gut microbiota (Liu et al., 2018). However, the chemical structures of pumpkin pectic polysaccharides are complex, and may be implicated in various immunomodulatory mechanisms. Moreover, little is known about the structure-activity relationships of pumpkin pectic polysaccharides or their mechanisms. To make more effective use of pumpkin resources, it is necessary to investigate the structure and immunomodulatory activity of pectic polysaccharides from *Cucurbita moschata* Duch. Therefore, we

hypothesized that pectic polysaccharides isolated from *Cucurbita moschata* Duch would exert an immunomodulatory effect.

In the current study, a pectic polysaccharide with immunomodulatory activity was isolated from *Cucurbita moschata* Duch and purified. The molecular weight and chemical structure of the obtained pectic polysaccharide fraction were determined. The immunoregulatory activity and possible mechanism of the pectic polysaccharide was investigated in vitro using a RAW 264.7 macrophage model. Our findings may contribute to understanding of the structure-activity relationship and the molecular mechanisms underlying the immunomodulatory activity of pumpkin pectic polysaccharide.

Table 1
Methylation analysis data for CMDP-4b.

Retention time	Methylated sugars	Mass fragments (<i>m/z</i>)	Molar ratios	Type of linkage
17.44	2,3,4,6-Me ₄ -Galp	43,71,87,101,117,129,145,161,205	0.056	GalpA-(1→
18.494	2,4-Me ₂ -Rhap	43,58,85,89,99,117,127,131,159,201	0.103	→3)-Rhap-(1→
20.97	2,3,6-Me ₃ -Galp	43,87,99,101,113,117,129,131,161,173,233	0.719	→4)-GalpA-(1→
24.764	2,6-Me ₂ -Galp	43,87,99,117,129,143	0.122	→3,4)-GalpA-(1→

2. Materials and methods

2.1. Materials

Fresh mature pumpkin (*Cucurbita moschata* Duch.) was obtained from a market in Beijing, China. Standard monosaccharides including arabinose (Ara), rhamnose (Rha), fucose (Fuc), ribose (Rib), *N*-acetyl-D-glucosamine (GlcNA), glucosamine hydrochloride (GlcN), galactose (Gal), xylose (Xyl), mannose (Man), D-galactosamine hydrochloride (GalN), fructose (Fru), glucuronic acid (GlcA), mannose acid (ManA), galacturonic acid (GalA), guluronic acid (GulA), and glucose (Glc) were supplied by Putian Tongchuang Biotechnology (Beijing, China). The DEAE cellulose-52 and Superdex-G200 were supplied by Yuanye Biotechnology (Shanghai, China). Cell line RAW 264.7 were obtained from ATCC. *Escherichia coli* (*E. coli*) was purchased from TransGen Biotech (Beijing, China). MTT assay kit was obtained by Solarbio Science & Technology (Beijing, China). Lipopolysaccharide (LPS) and neutral red were supplied by Sigma (USA). TNF- α , IL-1 β and IL-6 ELISA kits were supplied from R&D Systems (USA). The Pierce bicinchoninic acid protein assay kit and the nitrous oxide (NO) detection kit were supplied by Beyotime (Shanghai, China). The antibodies against MR, TLR2, TLR4, and CR3 were obtained from Abcam (USA). The antibodies against I κ B α , p38, p-ERK1/2, NF- κ B p65, p-p38, JNK, ERK1/2, p-JNK, β -actin, and Lamin B1 were supplied by Cell Signaling Technology (USA).

2.2. Extraction and purification of polysaccharide

Crude polysaccharide was isolated from pumpkin as previously reported (Song et al., 2015). In brief, pieces of pumpkin were pulped in a laboratory mill using distilled water as the extraction agent at a solid-liquid ratio of 1/4 (w/v). The mixture was heated at 80 °C for 4 h while stirring continuously. Following centrifugation, the proteins in the resultant supernatant were removed using Sevag reagent (1-butanol/chloroform; v/v = 1:4). Ethanol was added to the solution (80% final concentration), and a precipitate was formed over 12 h at 4 °C. The precipitate was recovered by centrifugation, dialyzed (membrane cut-off of 8000–1400 Da), and lyophilized to produce a crude polysaccharide named CMDP. Then purified sequentially using DEAE cellulose-52 anion exchange chromatography. Elutions of the column were carried out stepwise with ultrapure water (flow rate: 2 mL per min). Next, the eluent (CMDP-4) obtained from 0.3 M NaCl was loaded onto a Superdex G-200 column (flow rate: 1 mL per min). Finally, the major fraction, designated as CMDP-4b, was collected and lyophilized due to its high yield (Fig. 1A).

2.3. Characterization of CMDP-4b

2.3.1. Ultraviolet spectrum analysis

The ultraviolet absorbance of the CMDP-4b (1 mg/mL) solution was determined by a scanning spectrophotometer (U-2910, Japan) with a spectrum range of 200 to 350 nm.

2.3.2. Homogeneity and molecular mass analysis

According to a previously published method (Gou et al., 2019), HPGPC carried out for the analysis of molecular mass and homogeneity of CMDP-4b. HPGPC was performed by using Waters 2414 refractive

index detector and Waters 1525 HPLC system equipped with an Ultra-hydrogel™ Linear column. CMDP-4b (10 μ L; 1.0 mg/mL) was injected into the system for analysis using distilled water as the eluent at a flow rate of 0.9 mL/min. The molecular mass of CMDP-4b was determined by comparison with the retention time-molecular mass curve derived from a series of molecular mass standards (M_w = 1000, 5000, 12,000, 25,000, 50,000, and 150,000 Da).

2.3.3. FT-IR analysis

CMDP-4b sample was analyzed by FT-IR spectroscopy in a frequency region of 4000–400 cm^{-1} (Tianjing Gangdong Sci. & Tech., Tianjin, China) as previously mentioned (Shao et al., 2020). In brief, approximately 2 mg of CMDP-4b dried using phosphorus pentoxide was mixed with 200 mg of dried KBr powder and pressed into a 1 mm pellet for FT-IR analysis.

2.3.4. Determination of monosaccharide composition and degree of esterification (DE) and acetylation

The monosaccharide composition of CMDP-4b was determined by high-performance ion exchange chromatography (HPIEC) using a previously reported procedure (Shao et al., 2020). Briefly, 10 mg of CMDP-4b was hydrolyzed with 4 mL of 2 mol/L trifluoroacetic acid in a sealed ampoule bottle for 6 h at 110 °C, then evaporated under reduced pressure with 4 mL of methanol in a rotary vacuum evaporator. The hydrolyzed product was derivatized with 500 μ L of 0.5 mol/L methanol/1-phenyl-3-methyl-5-pyrazolone in alkaline conditions. The resultant CMDP-4b was analyzed using a Waters e 2695 high-performance liquid chromatography (HPLC) system, detected using a photodiode array (PDA) detector, and connected with an Athena WP-C18 column (4.6 \times 150 nm, 5 μ m). The analytical standards were Fuc, Rha, Ara, Glc, GlcNA, GlcN, Gal, Xyl, Man, GlcA, GalN, Fru, Rib, GalA, GulA, and ManA.

The degree of DE and acetylation of CMDP-4b was determined by the titrimetric method (USP 26 NF 108 21, 2003) and the hydroxylamine-ferric trichloride method (Notari & Munson, 1969), respectively.

2.3.5. Methylation analysis

As previously described by Ciucanu and Kerek (1984), methylation analysis was carried out as follow: CMDP-4b dry powder (5 mg) was dissolved in dimethylsulfoxide (0.5 mL) containing 20 mg NaOH. The permethylated materials were hydrolyzed with formic acid and 1 mL of 2 M trifluoroacetic acid, reduced with NaBH₄, and acetylated with acetic anhydride to produce their partially methylated alditol acetates. The resultant polysaccharides were transformed into partially methylated alditol acetates and analyzed using a GC-MS system (GCMS-QP2010 Plus; Shimadzu, Japan) with a TR-5MS capillary column (30 m \times 0.250 mm \times 0.25 μ m). The temperature program was as follows: the initial temperature of the column (150 °C) was increased to 180 °C at 10 °C/min, and subsequently to 260 °C at 15 °C/min.

2.3.6. Nuclear magnetic resonance (NMR) analysis

As previously published (Li et al., 2021), 100 mg CMDP-4b was dissolved in 1000 μ L of D₂O (99.9 atom%) at 25 °C and lyophilized. Subsequently, the CMDP-4b was re-dissolved in D₂O via a 0.22 μ m membrane before NMR analysis, and then transferred to a 5 mm NMR tube for testing. High-resolution ¹H and ¹³C NMR spectra were recorded at 600 MHz and 150 MHz, respectively, using a 5 mm inverse geometry ¹H/¹³C probe and a Bruker AV-600 spectrometer (Bruker, Rheinstetten,

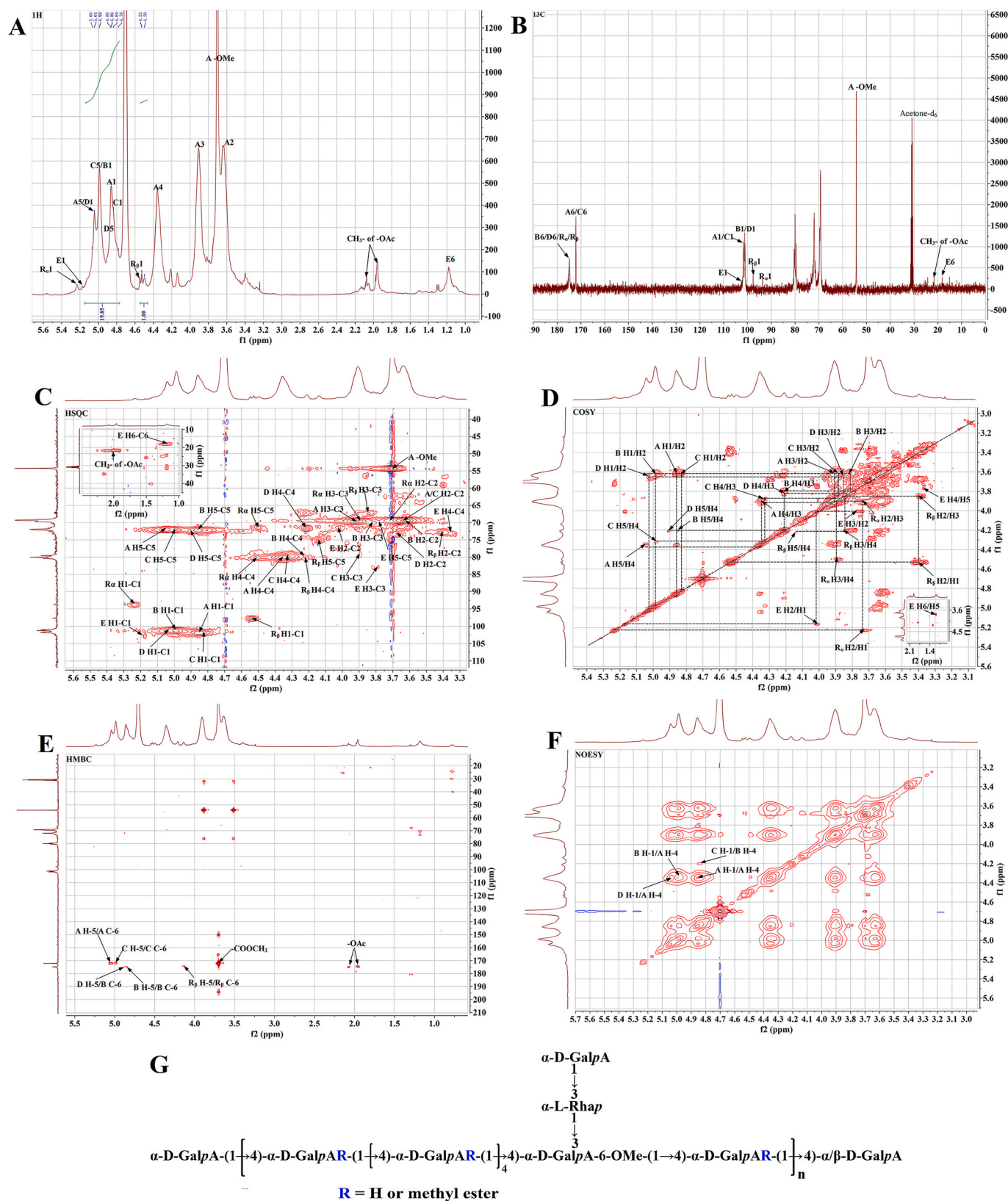


Fig. 2. (A) ^1H , (B) ^{13}C , (C) HSQC, (D) COSY, (E) HMBC, and (F) NOESY spectra of CMDP-4b in D_2O solution at 25 °C, (G) Putative structure of CMDP-4b.

Germany) at a temperature of 298 K. The correlation spectroscopy (COSY), heteronuclear single-quantum correlation spectroscopy (HSQC), heteronuclear multiple-bond correlation spectroscopy (HMBC), and nuclear Overhauser effect spectroscopy (NOESY) spectra were

obtained based on standard Bruker pulse sequences. Chemical shifts are presented in ppm, and were obtained using the internal acetone- D_6 signal ($\delta_{\text{H}} = 2.09$ ppm) for the ^1H spectra and the internal acetone- D_6 signal ($\delta_{\text{C}} = 30.89$ ppm) for the ^{13}C spectra as references. Data were

Table 2
¹H and ¹³C NMR chemical shifts (ppm) of CMDP-4b in D₂O.

Glycosyl residues			Chemical shift $\delta_{H/C}$ (ppm)						CH3-of-OMe
			1	2	3	4	5	6	
A	→4)-α-D-GalpA-6-OMe-(1→	H	4.86	3.64	3.90	4.35	5.05		3.70
		C	101.81	69.31	69.47	79.93	72.04	172.16	54.25
B	→4)-α-D-GalpA-(1→	H	4.99	3.62	3.82	4.21	4.86		
		C	101.24	69.46	69.75	79.36	71.84	174.81	
C	→3,4)-α-D-GalpA-6-OMe-(1→	H	4.83	3.61	3.88	4.32	4.98		3.70
		C	101.64	69.46	79.48	79.92	72.01	172.16	54.25
D	α-D-GalpA-(1→	H	5.03	3.66	3.85	4.21	4.90		
		C	101.36	72.85	69.46	71.44	72.29	174.81	
E	→3)-α-L-Rhap-(1→	H	5.18	4.01	3.78	3.35	3.77		1.18
		C	102.64	71.72	82.87	72.98	69.75	18.08	
R _α	→4)-α-D-GalpA	H	5.24	3.72	3.90	4.52	4.50		
		C	93.72	69.31	69.58	80.04	71.44	174.81	
R _β	→4)-β-D-GalpA	H	4.55	3.40	3.85	4.21	4.14		
		C	97.67	72.69	67.20	80.21	75.11	174.81	

analyzed using The MestRe Nova 5.3.0 software (Spain).

2.4. Immunoregulatory activity of CMDP-4b

2.4.1. Cell viability assessment

The RAW264.7 macrophages were treated with CMDP-4b (0, 62.5, 125, 250, or 500 µg/mL) for 24 h in 96-well plates. Then, MTT solutions (20 µL, 5 mg/mL) were incubated with the cell for 4 h. The absorbance of formazan was dissolved in 100 µL DMSO and measured (570 nm) using a multifunction microplate reader (Spark 20M).

2.4.2. Measurement of pinocytic activity

RAW264.7 macrophages (5×10^5 cells/well) were seeded in 96-well plates. Twenty-four hours later, LPS (1 µg/mL) or CMDP-4b at 62.5, 125, or 250 µg/mL was added to cells, and the macrophages were kept in 37 °C for 24 h. 0.1% neutral red (100 µL/well) was incubated with the macrophages for a further 2 h. Cell lysis solution (150 µL/well) was added. The macrophages were kept for a further 12 h at 37 °C before measuring absorbances at 570 nm.

2.4.3. Measurement of phagocytic activity

Macrophages were seeded in 6-well plates (5×10^5 cells/mL), followed by 24-h incubation with LPS (1 µg/mL) or CMDP-4b at 62.5, 125, or 250 µg/mL. Then, suspensions of fluorescein isothiocyanate (FITC)-labeled *E. coli* were incubated with the cell for 2 h. For the determination of phagocytosis, 100 µL trypan blue suspensions were incubated for 1 min. The excessed trypan blue suspensions were removed and the fluorescence intensities of the macrophages were measured by flow cytometry.

2.4.4. Secretion of NO and cytokines

RAW 264.7 macrophages were treated with CMDP-4b (62.5, 125, or 250 µg/mL), or LPS (1 µg/mL) for 24 h. NO contents were tested by NO detection kit. The productions of IL-6, IL-1β and TNF-α were tested by ELISA.

2.4.5. Investigation of receptors on macrophages

Macrophages were pretreated with 5 µg/mL of antibodies against membrane receptors (TLR2, CR3, MR, or TLR4) or mixed antibodies (TLR2, CR3, MR and TLR4) for 2 h prior to the treatment with 250 µg/mL of CMDP-4b fractions. Twenty-four hours later, the supernatants were collected. Moreover, the levels of IL-6, TNF-α, and NO were determined as aforementioned.

2.4.6. Western blot

The macrophages were seeded on 60 mm² culture dishes (1×10^5 cells/well), and stimulated with LPS (1 µg/mL) or CMDP-4b (0, 62.5, 125, or 250 µg/mL) for 24 h. Western blot was performed as previously

reported (Qin et al., 2018). The membrane was blocked in blocking buffer for 2 h, next, the incubation with specific primary antibodies (p-ERK1/2, IκBα, p38, ERK1/2, p-p38, JNK, NF-κB p65, p-JNK, β-actin, and Lamin B1) at 4 °C overnight. Followed by the membrane was incubated with a secondary antibody for 2 h at 25 °C. The enhanced chemiluminescence reagent was used to visualize protein bands. The Omega Lum G imaging system (USA) and the Image Lab™ software was used to analyze the relative expression of proteins.

2.5. Statistical analysis

The means and standard deviations were obtained using the SPSS software (IBM Corporation, Armonk, NY, USA). Graphs were plotted using the Origin 8.5 software (Microcal, Northampton, MA, USA). One-factor analysis of variance (ANOVA) was carried out for each parameter. Mean values were considered significantly different when $p < 0.05$.

3. Results and discussion

3.1. CMDP-4b isolation and purification

The main polysaccharide fraction (CMDP-4; 40.6% yield) was further purified using a Superdex G-200 column. Then the main fraction of white flocculent polysaccharide (84.9% yield) obtained after dialysis, concentration, and lyophilization was designated CMDP-4b. As shown in Fig. 1B, CMDP-4b appeared as a single and symmetrical sharp peak, suggesting that CMDP-4b may be a homogeneous polysaccharide.

3.2. Characterization of CMDP-4b

3.2.1. UV-vis analysis, molecular mass, monosaccharide composition, and degree of DE and acetylation

CMDP-4b demonstrated no absorption at both 260 and 280 nm in the UV-vis spectrum (Fig. 1C), suggesting that it contained no nucleic acid or protein. The homogeneity of CMDP-4b was confirmed by HPGPC, which displayed a symmetrical polysaccharide peak at 40.48 min elution time (Fig. 1D). The molecular mass of CMDP-4b was estimated to be 31.97 kDa. Furthermore, compared with standard monosaccharides, CMDP-4b consisted of large amounts of galacturonic acid and low amounts of rhamnose, galactose, and arabinose at a weight ratio of 81.2:8.1:4.6:6.1, as shown in Fig. 1F. The composition of CMDP-4b was similar to that of other pectic polysaccharides extracted from *Cucurbita moschata* Duch. (Zhao et al., 2017), except for higher galacturonic acid content in CMDP-4b. The discrepancies in monosaccharide composition may be due to differences in the extraction methods used in different studies. Moreover, the DE and acetyl content of CMDP-4b was determined to be 89.4% and 3.2%, respectively. The endotoxin content of CMDP-4b was confirmed to be less than 0.25 EU/mL. These results

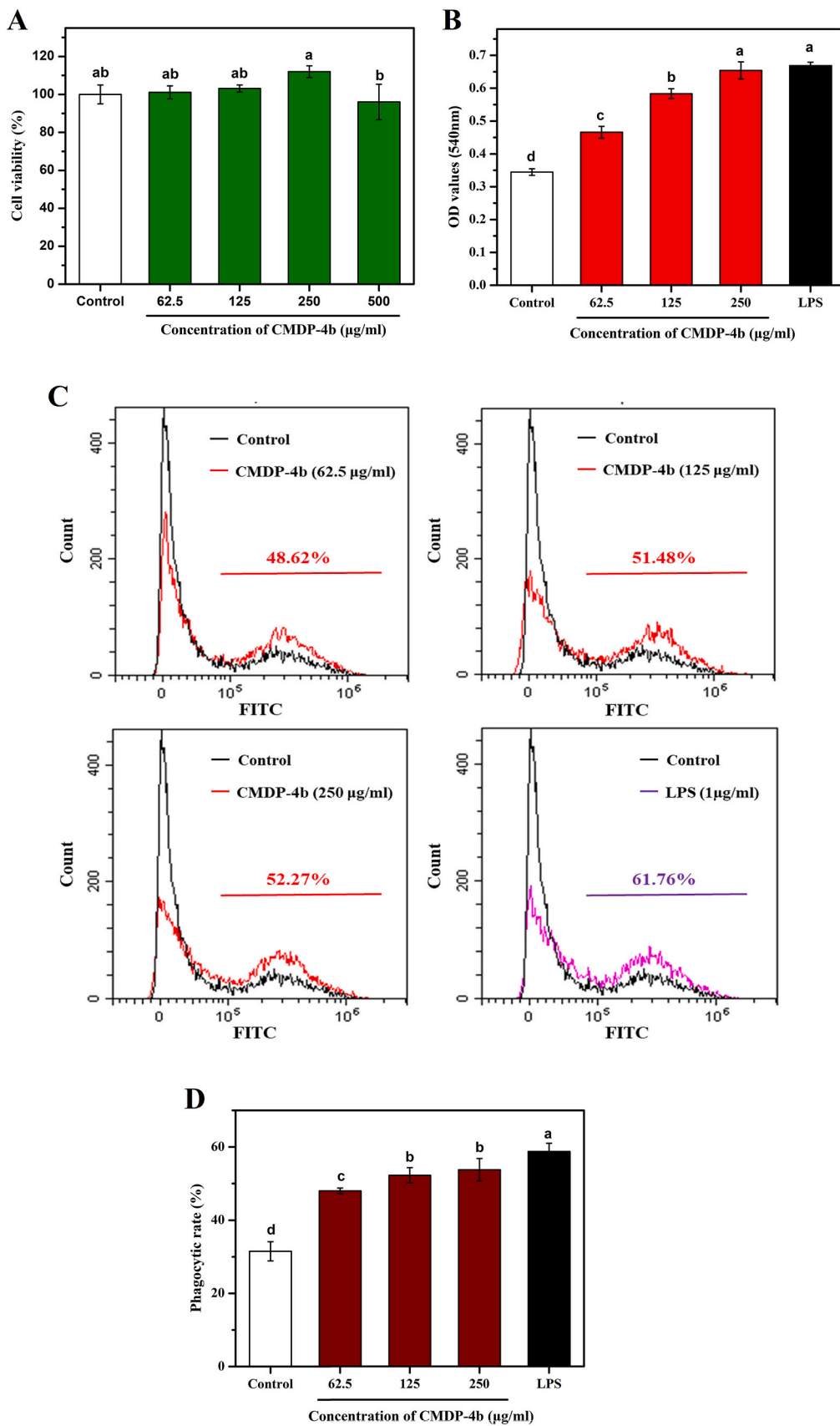


Fig. 3. (A) Effect of CMDP-4b on the viability of macrophages. (B) Effect of CMDP-4b on neutral red uptake by macrophages. (C) Fluorescence intensity of macrophages phagocytosing FITC-labeled *E. coli*. (D) Effect of CMDP-4b on the phagocytic rate of macrophages. Negative control, untreated macrophages; positive control, macrophages treated with LPS (1 μg/mL). Data are mean ± SD (n = 3). Different letters indicate significant differences among groups (p < 0.05).

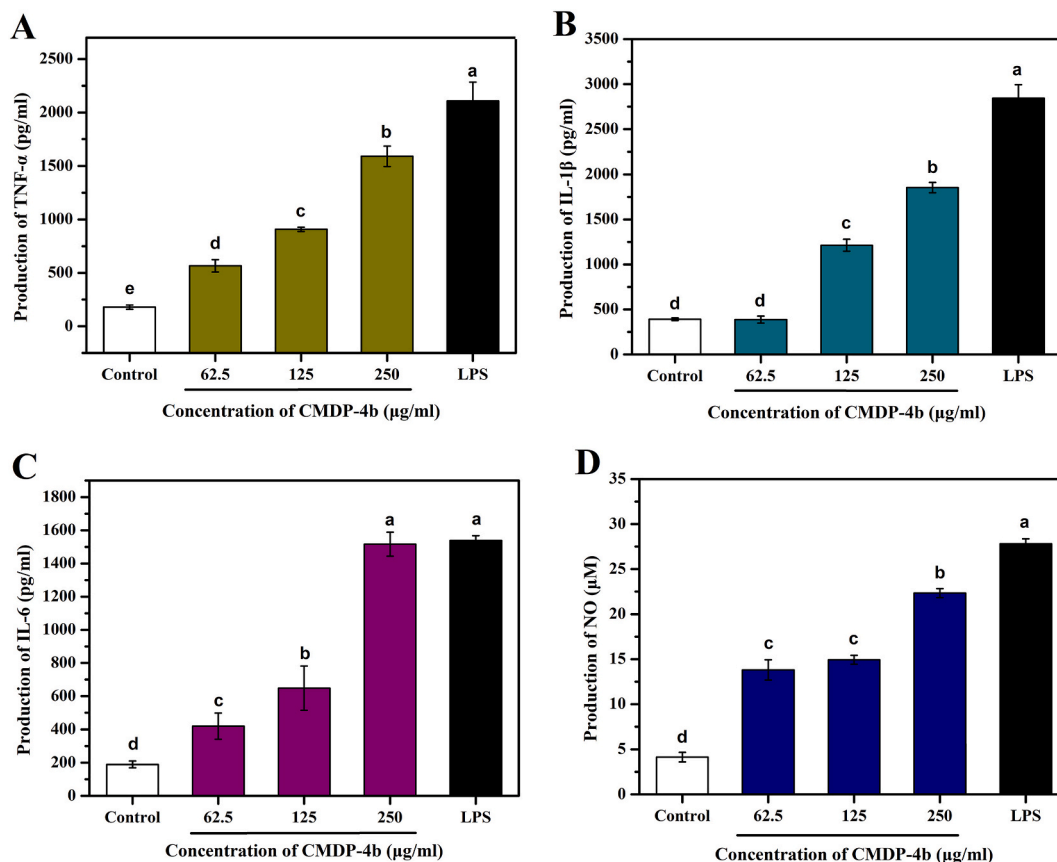


Fig. 4. Effects of CMDP-4b on the secretion of (A) TNF- α , (B) IL-1 β , (C) IL-6, and (D) NO from macrophages. Negative control, untreated macrophages; positive control, macrophages treated with LPS (1 μ g/mL). Data are mean \pm SD ($n = 3$). Different letters indicate significant differences among groups ($p < 0.05$).

suggested that CMDP-4b was a composition typical of pectic polysaccharide.

3.2.2. FT-IR analysis

As demonstrated in the Fig. 1E, in the result of FT-IR spectrum of CMDP-4b, one broad and intense peak was found at 3438 cm^{-1} , which was suggested to be hydroxyl stretching vibration. Absorption at 2927 cm^{-1} was assigned to the C-H stretching vibration of the polysaccharide (Wang et al., 2019). The band at 1739 cm^{-1} was characteristic of a uronic acid. The absorption at 1616 cm^{-1} was indicative of the stretch vibration of the -COO- of uronic acid (Zhana et al., 2018). The absorption at 1436 cm^{-1} indicated the presence of the C-O stretching vibration (Liu et al., 2016). The bands at 1145 cm^{-1} and 1020 cm^{-1} were suggested to the C-O-H and C-O-C. One absorption at 831 cm^{-1} indicated α -type glycosidic linkage (Miao et al., 2014). The bands at 763 cm^{-1} and 931 cm^{-1} were also observed, suggesting the presence of a pyranose ring (Zhao et al., 2005).

3.2.3. Methylation analysis

The glycosidic linkage types of reduced CMDP-4b included GalpA-(1 \rightarrow , \rightarrow 3)-Rhap-(1 \rightarrow , \rightarrow 4)-GalpA-(1 \rightarrow , and \rightarrow 3,4)-GalpA-(1 \rightarrow with a molar ratio of 5.6:10.3:71.9:12.2 (Table 1). These findings indicated that CMDP-4b mainly contained 1,4-linked GalpA in the backbone, while had a branch attached to the backbone at the 3-position. These results further imply that CMDP-4b may be a pectin-type polysaccharide (Chan et al., 2017). The structure of CMDP-4b was further detailed by 1D and 2D NMR analysis.

3.2.4. 1D and 2D NMR analysis

Based on ^1H NMR (Fig. 2A), ^{13}C NMR (Fig. 2B), and cross-peaks in HSQC spectrum (Fig. 2C), CMDP-4b exhibited seven anomeric proton

signals at δ 4.86, 4.99, 4.83, 5.03, 5.18, 5.24, and 4.55 ppm. The corresponding anomeric carbon signals were at δ 101.81, 101.24, 101.64, 101.36, 102.64, 93.72, and 97.67 ppm (labeled as A, B, C, D, E, R α , and R β , respectively). Chemical shifts of anomeric proton and carbon signals were completely assigned using 2D NMR spectrum analysis (Table 2) (Li et al., 2021; Yang et al., 2018; Zhao et al., 2017).

As shown in Fig. 2A and B, the carbon signal at δ 21.23 ppm and the proton signals at δ 1.96 and 2.08 ppm indicated the presence of the acetyl group in CMDP-4b (Perrone et al., 2002). The signals at δ 1.96/21.23 ppm and δ 2.08/21.23 ppm (Fig. 2C), and the peaks at δ 1.96/174.81 ppm and δ 2.08/174.81 ppm (Fig. 2E) were weak, suggesting a low degree of acetylation in CMDP-4b. The signals at δ 172.16 ppm in the HMBC spectrum, and stronger signal peaks at δ 3.70 and 54.25 ppm in ^1H NMR and ^{13}C NMR spectra inferred the presence of a methyl ester group in galacturonic acid residues.

The intensive anomeric carbon and proton signal of residue A was found at δ 101.81 ppm (C-1) and δ 4.86 ppm (H-1) (Fig. 2B and C), indicating the α -linkage of residue A. The cross-peaks in the COSY spectrum suggested that the chemical shifts from H-2 to H-5 were at δ 3.64, 3.90, 4.35, and 5.05 ppm, respectively (Fig. 2D). The corresponding ^{13}C chemical shifts of carbon were at δ 69.31, 69.47, 79.93, and 72.04 ppm for C-2 to C-5, respectively. Down-field chemical shift of C-1 and C-4 proved the presence of (1 \rightarrow 4)-linkages. The appearance of intra residual couplings at δ 172.16/4.98 ppm (C6/H5) and δ 172.16/3.70 ppm (C6/carboxy methyl proton) (Fig. 2E) suggested that the carboxyl group of galacturonic acid was esterified. Therefore, residue A was assigned to be \rightarrow 4)- α -D-GalpA-6-OMe-(1 \rightarrow (Patra et al., 2013). Likewise, residue C was determined to be \rightarrow 3,4)- α -D-GalpA-6-OMe-(1 \rightarrow with the C-1/H-1 (δ 101.64/4.89 ppm), C-2/H-2 (δ 69.46/3.52 ppm), C-3/H-3 (δ 79.48/3.63 ppm), C-4/H-4 (δ 79.92/3.34 ppm), and C-5/H-5 (δ 72.01/3.95 ppm) found in the HSQC and COSY spectra, with the

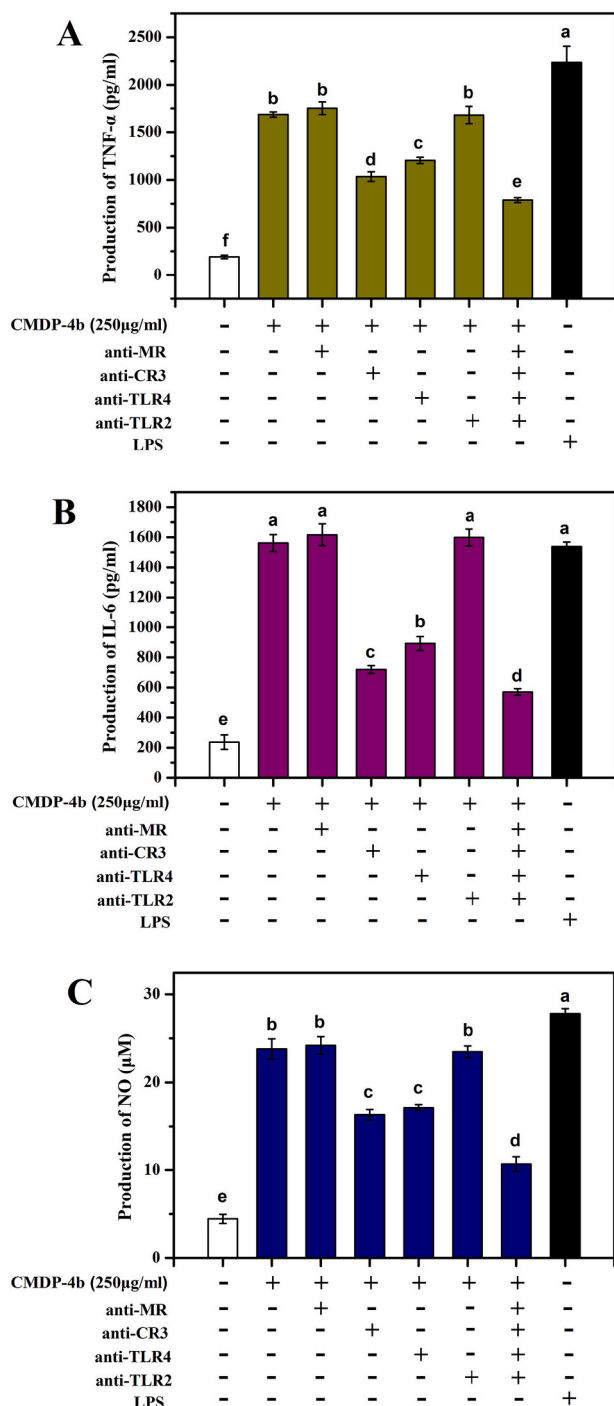


Fig. 5. Roles of MR, CR3, TLR2, and TLR4 in CMDP-4b-induced secretion of (A) TNF- α , (B) IL-6, and (C) NO from macrophages. Negative control, untreated macrophages; positive control, macrophages treated with LPS (1 μ g/mL). Data are mean \pm SD ($n = 3$). Different letters indicate significant differences among groups ($p < 0.05$).

downfield shift in the C-1, C-3, and C-4. Residue C showed H-5 (δ 5.05 ppm) with C-6 (δ 172.16 ppm) correlated to the protons of the methyl group (δ 3.70 ppm), indicating that the carboxyl group of galacturonic acid proved the presence of methyl ester.

For residue B, chemical shifts from H-1 to H-5 were assigned by the COSY (Fig. 2D) spectrum (δ 4.99, 3.62, 3.82, 4.21, and 4.86 ppm, respectively). The chemical shifts C-1, C-2, C-3, C-4, C-5 obtained from the HSQC spectrum were δ 101.24, 69.46, 69.75, 79.36, and 71.84 ppm, respectively. The cross-peak at δ 4.86/174.81 ppm was assigned as H5/

C6 in the HMBC spectrum (Fig. 3E), including C-6 chemical shift at δ 174.81 ppm and downfield shift in the C-1 and C-4 of residue B. Residue B was assigned to be \rightarrow 4)- α -D-GalpA-(1 \rightarrow) (Li et al., 2021). In terms of residue D, proton chemical shifts from H-1 to H-5 (δ 5.03, 3.66, 3.85, 4.21, and 4.90 ppm) were assigned by the COSY spectrum (Fig. 3D). The 13 C assignments of residue D were tested by HSQC and HMBC spectra (Fig. 3C and E; Table 2) and the downfield of the C-1 allowed the assignment of residue D as α -D-GalpA-(1 \rightarrow) (Zhang et al., 2016). The chemical shifts of residue E from H-1 to H-6 were at δ 5.01, 4.01, 3.78, 3.35, 3.77, and 1.18 ppm, respectively (Fig. 3D). Moreover, the matching 13 C chemical shifts were identified in the HSQC spectrum (Fig. 3C; Table 2), implying that residue E was \rightarrow 3)- α -L-Rhap-(1 \rightarrow) (Zhang et al., 2019).

Except for general residues (A, B, C, D, and E), two specific peaks at δ 5.24 and 4.55 ppm (designated as residue R $_{\alpha}$ and R $_{\beta}$, respectively) were present in the 1 H NMR spectrum (Fig. 1A). Their corresponding anomeric carbons were δ 93.72, 97.67 ppm (Fig. 2C), indicating that residue R $_{\alpha}$ and R $_{\beta}$ contained both α - and β -configurations (Zhu et al., 2019). The chemical shifts of residue R $_{\alpha}$ from H-1 to H-5 were tested by the COSY spectrum (δ 5.24, 3.72, 3.90, 4.52, and 4.50 ppm, respectively) (Fig. 2D). The 13 C chemical shifts were obtained using the HSQC spectrum (Table 2). Likewise, for residue R $_{\beta}$, the signals at δ 4.55/97.67, 3.40/72.69, 3.85/67.20, 4.21/80.21, 4.14/75.11, and 174.81 ppm were identified to H1/C1, H2/C2, H3/C3, H4/C4, H5/C5, and C6, respectively. The downfield resonances of the C-4 confirmed that residue R $_{\alpha}$ and R $_{\beta}$ were assigned to be \rightarrow 4)- α -D-GlapA and \rightarrow 4)- β -D-GlapA, respectively (Mutallifu et al., 2020).

In the NOESY spectrum (Fig. 2F), the intra-residual cross peak between H-4 (δ 4.35 ppm) and H-1 (δ 4.86 ppm) of residue A indicated the α -1,4-linkage between residue A and residue A. The cross-peak between H-1 (δ 4.99 ppm) of residue B and H-4 (δ 4.35 ppm) of residue A, H-4 (δ 4.35 ppm) of residue A and H-1 (δ 5.03 ppm) of residue D, and H-4 (δ 4.21 ppm) of residue B and H-1 (δ 4.83 ppm) of residue C indicated that residue A was linked to residue B; residue A was linked to residue D; residue B was linked to residue C, respectively. The molar ratio of residues obtained from methylation analysis and the above spectrum analysis indicate that the backbone of CMDP-4b was linked through an α -1,4-linkage between residue A and residue B. Taken together, these results proved that other residues linked to the backbone at C-3, suggesting that CMDP-4b was composed of repeating units. The possible structure of CMDP-4b is shown in Fig. 2G.

3.3. Immunomodulatory effect of CMDP-4b on macrophages

3.3.1. Effect of CMDP-4b on the viability of macrophages

CMDP-4b was not toxic to macrophages within a certain concentration range (62.5–250 μ g/mL). CMDP-4b at 125 and 250 μ g/mL significantly enhanced the viability of RAW 264.7 macrophages compared to the control group ($p < 0.05$) (Fig. 3A). However, CMDP-4b exerted significant suppressive effects on macrophages at 500 μ g/mL ($p < 0.05$). Therefore, CMDP-4b at 62.5, 125, and 250 μ g/mL was used in subsequent experiments.

3.3.2. Effect of CMDP-4b on pinocytotic and phagocytotic activities of macrophages

RAW264.7 macrophage was pre-treated with CMDP-4b in different concentrations, and the pinocytotic activity of the macrophages was tested through monitoring the uptake of neutral red. As a result, comparing with the negative control group, RAW264.7 macrophages treated with CMDP-4b (62.5, 125, and 250 μ g/mL) showed significantly stimulated pinocytotic activity in dose-dependent manner ($p < 0.05$) (Fig. 3B), suggesting that CMDP-4b enhanced macrophage pinocytosis to increase their immunomodulatory effect.

The impacts of CMDP-4b on the phagocytotic activity of macrophages were analyzed by monitoring the uptake of *E. coli*. The fluorescence intensity of macrophages phagocytosing FITC-labeled *E. coli* was

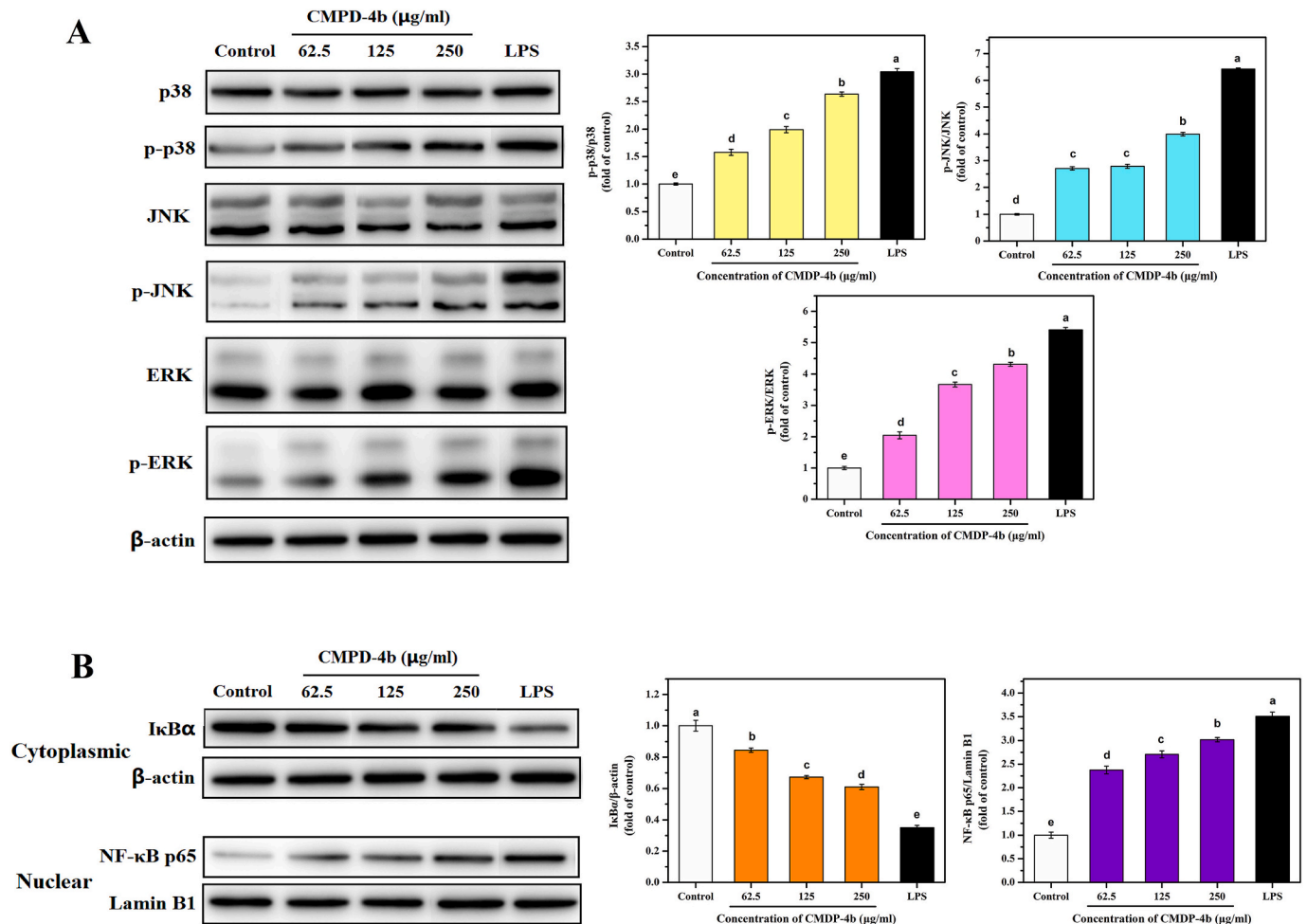


Fig. 6. Effects of CMDP-4b on the MAPKs and the NF- κ B signaling pathways in macrophages. (A) Representative blot images and quantitative analysis of the levels of p-p38/p38, p-pJNK/JNK, and p-ERK/ERK. (B) Representative blot images and quantitative analysis of the levels of NF- κ B p65 and κ B α . Negative control, untreated macrophages; positive control, macrophages treated with LPS (1 μ g/mL). The values were normalized to the negative control group. Data are mean \pm SD ($n = 3$). Different letters indicate significant differences among groups ($p < 0.05$).

determined by flow cytometer (Fig. 3C). The phagocytic rate further confirmed the results of flow cytometry (Fig. 3D). With increasing concentrations of CMDP-4b up to 250 μ g/mL, the phagocytic capacity increased rapidly. However, the stimulatory effect of CMDP-4b at the highest concentration on the phagocytic rate of macrophages was not stronger than that of 1 μ g/mL LPS ($p < 0.05$). The over-activation of macrophages has been shown to cause inflammatory damage (Sica & Mantovani, 2012). The fluorescence microscope was then used to further confirm the result (Fig. A.2). The images reveal that the fluorescence intensity due to the macrophages treated with CMDP-4b or LPS was obviously stronger than in the control group. Our results revealed the immunomodulatory effect of CMDP-4b, which was beneficial for resisting foreign pathogen invasion by moderately promoting the phagocytic activity of macrophages.

3.3.3. Effects of CMDP-4b on the production of NO and cytokines in macrophages

Upon pathological stimulation or injury, activated macrophages produce NO and cytokines to augment innate immune responses (Lee & Jeon, 2005). As shown in Fig. 4, the secretions of NO and all cytokines from RAW264.7 macrophages increased as the concentration of CMDP-4b from 62.5 to 250 μ g/mL. Compared to the macrophages treated with LPS, those treated with 250 μ g/mL CMDP-4b released much less NO, IL-1 β , and TNF- α , indicating that CMDP-4b moderately increased the secretion of cytokines and NO from macrophages without inducing

macrophage apoptosis. The stimulatory effects of CMDP-4b on the production of NO and cytokines suggested that CMDP-4b effectively activated macrophages.

3.3.4. Receptors of CMDP-4b on macrophages

The activation of macrophages is initiated by the stimulation of pattern recognition receptors (Kumar, 2019). As shown in Fig. 5A–C, CMDP-4b-induced secretion of IL-6, TNF- α , and NO from macrophages was significantly decreased by the treatment with anti-CR3 or anti-TLR4 antibodies ($p < 0.05$). However, when macrophages were treated with anti-TLR2 or anti-MR antibodies, the release of TNF- α , IL-6, and NO levels were not significantly differently from that of 250 μ g/mL CMDP-4b group. The production of TNF- α , IL-6, and NO in macrophages dealt with mixed antibodies were significantly different from that in negative control group ($p < 0.05$). These data indicated that CR3 and TLR4 were major receptors of CMDP-4b. However, the possibility of the existence of other receptors could not be excluded.

3.3.5. Effects of CMDP-4b on the signaling pathways in macrophages

To determine whether the MAPKs and the NF- κ B signaling pathways were related to the activation of macrophages by CMDP-4b, we treated macrophages with different concentrations of CMDP-4b or LPS (1 μ g/mL). As shown in Fig. 6A, CMDP-4b at 62.5–250 μ g/mL significantly and concentration-dependently increased phosphorylation of MAPKs (JNK, ERK, and p38). However, the total MAPKs levels were not affected by

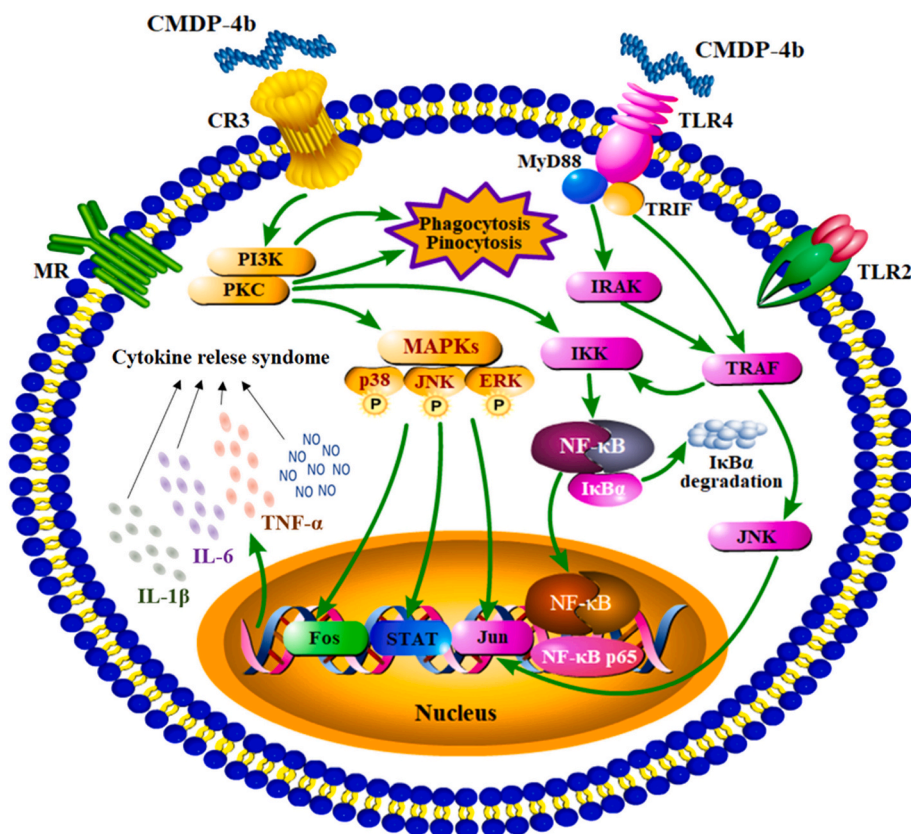


Fig. 7. Possible signal transduction pathways involved in the activation of macrophages by CMDP-4b.

CMDP-4b stimulation. Moreover, CMDP-4b-treated macrophages showed a significant and dose-dependent increase in the protein levels of NF- κ B p65 in comparison to negative control group ($p < 0.05$). Additionally, the I κ B α protein was degraded in macrophages induced by CMDP-4b (Fig. 6B). These findings indicated that the MAPKs and the NF- κ B signaling pathways were related to the activation of macrophages by CMDP-4b. Furthermore, pre-treatment with pyrrolidine dithiocarbamate (PDTC, NF- κ B inhibitor), SB203580 (p38 inhibitor), SP600125 (JNK inhibitor), and PD98059 (MAPKK inhibitor) significantly suppressed increases in TNF- α , IL-6, and NO production induced by CMDP-4b ($p < 0.05$), as shown in Fig. A.3. The results also suggest that CMDP-4b-induced macrophage activation occurs via NF- κ B and MAPKs signaling pathways.

3.3.6. Possible molecular mechanisms of CMDP-4b-induced activation of macrophages

Based on previous findings (Schepetkin & Quinn, 2006) and the above results, we present a schematic diagram of potential mechanisms underlying the immunomodulatory activity of CMDP-4b (Fig. 7). As aforementioned discussed, CMDP-4b activates macrophages via acting with CR3 and TLR4. TLR4 recognizes the structure of polysaccharides and then activates myeloid differentiation protein 88 via an adaptor, IL-1 receptor-associated kinase, followed by the activation of TNF receptor-associated factor, MAPKs, and NF- κ B. Meanwhile, CR3 activates phosphoinositide-3-kinase and protein kinase C, which then trigger the activation of intracellular signaling pathways (i.e. MAPKs and NF- κ B) and therefore increase the phagocytic and pinocytic activities of macrophages. Ultimately, these pathways lead to induce the release of IL-1 β , TNF- α , IL-6, and NO. Therefore, the immunomodulatory activity of CMDP-4b may mainly be driven by the activation of these signaling pathways. Studies have confirmed that pectic polysaccharides have immunostimulatory activities, both in vitro and in vivo. However, the immunomodulatory activities and mechanisms of operation differ

among pectic polysaccharides with particular physicochemical properties and structural characteristics (Minzanova et al., 2018; Zhang et al., 2018). Pectic polysaccharides from *Zizyphus jujuba cv. Junzao* with backbones comprising linear chains of α -1,4-D-galacturonan have potential immunomodulatory effects, they increase the levels of cytokines in macrophages (Zhana et al., 2018). It should be noted that specific structural regions have a great influence on macrophage activation. The immunomodulatory activity of a polysaccharide from *Lemna minor* L. disappeared after removal of the linear 1,4-D-galactopyranosyluronan regions (Popov et al., 2006). In addition, polysaccharides in the molecular weight range 10–1000 kDa are more effective at adjusting immune function (Schepetkin & Quinn, 2006). Therefore, the immunostimulatory activity of CMDP-4b might be related to its molecular weight (31.97 kDa) and its dominant α -1,4-D-galacturonan residues.

4. Conclusion

In summary, a pectic polysaccharide (CMDP-4b) from *Cucurbita moschata* Duch was isolated, purified and characterized. CMDP-4b had a molecular weight of 31.97 kDa, and its repeating unit structure was proposed as described above. Moreover, CMDP-4b exhibited immunomodulatory activity by enhancing pinocytosis and phagocytosis of macrophages and promoting the production of cytokines and NO via acting with TLR4 and CR3 on cell surface, thereby activating the MAPKs and the NF- κ B signaling pathways. Collectively, CMDP-4b could potentially be used as a potential immunostimulant for patients with hyp immunity.

CRedit authorship contribution statement

Linlin Huang: Conceptualization, Methodology, Formal analysis, Writing – original draft, Writing – review & editing. **Jing Zhao:**

Supervision, Writing – original draft. **Yunlu Wei**: Data curation, Writing – review & editing. **Guoyong Yu**: Investigation, Validation. **Fei Li**: Project administration. **Quanhong Li**: Supervision, Writing – review & editing, Funding acquisition, Data curation.

Declaration of competing interest

The authors declare no conflict of interest.

Acknowledgement

This project was supported by the opening fund of Beijing Advanced Innovation Center for Food Nutrition and Human Health.

Appendix A. Supplementary data

Supplementary data to this article can be found online at <https://doi.org/10.1016/j.carbpol.2021.118288>.

References

- Chan, S. Y., Choo, W. S., Young, D. J., & Loh, X. J. (2017). Pectin as a rheology modifier: Origin, structure, commercial production and rheology. *Carbohydrate Polymers*, *161*, 118–139.
- Chen, L., & Huang, G. (2019). Antioxidant activities of phosphorylated pumpkin polysaccharide. *International Journal of Biological Macromolecules*, *125*, 256–261.
- Ciucanu, I., & Kerek, F. (1984). A simple and rapid method for the permethylation of carbohydrates. *Carbohydrate Research*, *131*(2), 209–217.
- Gou, Y., Sun, J., Liu, J., Chen, H., Kan, J., Qian, C., Zhang, N., & Jin, C. (2019). Structural characterization of a water-soluble purple sweet potato polysaccharide and its effect on intestinal inflammation in mice. *Journal of Functional Foods*, *61*, Article 103502.
- Kanmani, P., Albarracin, L., Kobayashi, H., Iida, H., Komatsu, R., Kober, A. K. M. H., ... Kitazawa, H. (2018). Exopolysaccharides from *Lactobacillus delbrueckii* OLL1073R-1 modulate innate antiviral immune response in porcine intestinal epithelial cells. *Molecular Immunology*, *93*, 253–265.
- Kumar, V. (2019). The complement system, toll-like receptors and inflammasomes in host defense: Three musketeers' one target. *International Reviews of Immunology*, *38*(4), 131–156.
- Lee, K. Y., & Jeon, Y. J. (2005). Macrophage activation by polysaccharide isolated from *Astragalus membranaceus*. *International Immunopharmacology*, *5*(7–8), 1225–1233.
- Li, F., Wei, Y., Liang, L., Huang, L., Yu, G., & Li, Q. (2021). A novel low-molecular-mass pumpkin polysaccharide: Structural characterization, antioxidant activity, and hypoglycemic potential. *Carbohydrate Polymers*, *251*, Article 117090.
- Liu, G., Liang, L., Yu, G., & Li, Q. (2018). Pumpkin polysaccharide modifies the gut microbiota during alleviation of type 2 diabetes in rats. *International Journal of Biological Macromolecules*, *115*, 711–717.
- Liu, X. C., Zhu, Z. Y., Tang, Y. L., Wang, M. F., Wang, Z., Liu, A. J., & Zhang, Y. M. (2016). Structural properties of polysaccharides from cultivated fruit bodies and mycelium of *Cordyceps militaris*. *Carbohydrate Polymers*, *142*, 63–72.
- Maran, J. P., Mekala, V., & Manikandan, S. (2013). Modeling and optimization of ultrasound-assisted extraction of polysaccharide from *Cucurbita moschata*. *Carbohydrate Polymers*, *92*, 2018–2026.
- Martinez, F. O., Helming, L., & Gordon, S. (2009). Alternative activation of macrophages: An immunologic functional perspective. *Annual Review of Immunology*, *27*, 451–483.
- Miao, M., Ma, Y., Jiang, B., Huang, C., Li, X., Cui, S. W., & Zhang, T. (2014). Structural investigation of a neutral extracellular glucan from *Lactobacillus reuteri* SK24.003. *Carbohydrate Polymers*, *106*, 384–392.
- Minzanova, S. T., Mironov, V. F., Arkhipova, D. M., Khabibullina, A. V., Mironova, L. G., Zakirova, Y. M., & Milyukov, V. A. (2018). Biological activity and pharmacological application of pectic polysaccharides: A review. *Polymers*, *10*(12), 1407.
- Mutallifu, P., Bobakulov, K., Abuduwaili, A., Huojiaihemaiti, H., Nuexiati, R., Aisa, H. A., & Yili, A. (2020). Structural characterization and antioxidant activities of a water soluble polysaccharide isolated from *Glycyrrhiza glabra*. *International Journal of Biological Macromolecules*, *144*, 751–759.
- Notari, T., & Munson, J. W. (1969). Hydroxamic acids. I. Factors affecting the stability of the hydroxamic acid-iron complex. *Journal of Pharmaceutical Sciences*, *58*, 1060–1064.
- Patra, P., Sen, I. K., Bhanja, S. K., Nandi, A. K., Samanta, S., Das, D., ... Islam, S. S. (2013). Pectic polysaccharide from immature onion stick (*Allium cepa*): Structural and immunological investigation. *Carbohydrate Polymers*, *92*(1), 345–352.
- Perrone, P., Hewage, C. M., Thomson, A. R., Bailey, K., Sadler, I. H., & Fry, S. C. (2002). Patterns of methyl and O-acetyl esterification in spinach pectins: New complexity. *Phytochemistry*, *60*(1), 67–77.
- Popov, S. V., Ovodova, R. G., & Ovodov, Y. S. (2006). Effect of lemnian, pectin from *Lemna minor* L., and its fragments on inflammatory reaction. *Phytotherapy Research*, *20*(5), 403–407.
- Qin, D., Li, L., Li, J., Li, J., Zhao, D., Li, Y., ... Zhang, X. (2018). A new compound isolated from the reduced ribose-tryptophan maillard reaction products exhibits distinct anti-inflammatory activity. *Journal of Agricultural and Food Chemistry*, *66*(26), 6752–6761.
- Schepetkin, I. A., & Quinn, M. T. (2006). Botanical polysaccharides: Macrophage immunomodulation and therapeutic potential. *International Immunopharmacology*, *6*(3), 317–333.
- Shao, X., Sun, C., Tang, X., Zhang, X., Han, D., Liang, S., ... Chen, C. (2020). Anti-inflammatory and intestinal microbiota modulation properties of Jinxiang garlic (*Allium sativum* L.) polysaccharides toward dextran sodium sulfate-induced colitis. *Journal of Agricultural and Food Chemistry*, *68*(44), 12295–12309.
- Sica, A., & Mantovani, A. (2012). Macrophage plasticity and polarization: In vivo veritas. *Journal of Clinical Investigation*, *122*(3), 787–795.
- Song, Y., Zhao, J., Ni, Y. Y., & Li, Q. H. (2015). Solution properties of a heteropolysaccharide extracted from pumpkin (*Cucurbita pepo*, lady godiva). *Carbohydrate Polymers*, *132*, 221–227.
- USP 26 NF 21. (2003). *The United States pharmacopeia-The national formulary* (Vol. 383, pp. 1401–1402). Rockville, MD: United States Pharmacopeial Convention.
- Wang, S., Zhao, L., Li, Q., Liu, C., Han, J., Zhu, J., Zhu, D., He, Y., & Liu, H. (2019). Rheological properties and chain conformation of soy hull water-soluble polysaccharide fractions obtained by gradient alcohol precipitation. *Food Hydrocolloids*, *91*, 34–39.
- Yadav, M., Jain, S., Tomar, R., Prasad, G. B., & Yadav, H. (2010). Medicinal and biological potential of pumpkin: An updated review. *Nutrition Research Reviews*, *23*(2), 184–190.
- Yang, J., Wen, L., Zhao, Y., Jiang, Y., Tian, M., Liu, H., Liu, J., & Yang, B. (2018). Structure identification of an arabinogalacturonan in *Citrus reticulata* Blanco 'Chachiensis' peel. *Food Hydrocolloids*, *84*, 481–488.
- Zhana, R., Xiab, L., Shaoc, J., Wanga, C., & Chen, D. (2018). Polysaccharide isolated from Chinese jujube fruit (*Zizyphus jujuba* cv. *Junzao*) exerts anti-inflammatory effects through MAPK signaling. *Journal of Functional Foods*, *40*, 461–470.
- Zhang, Q., Xu, Y., Lv, J., Cheng, M., Wu, Y., Cao, K., Zhang, X., Mou, X., & Fan, Q. (2018). Structure characterization of two functional polysaccharides from *Polygonum multiflorum* and its immunomodulatory. *International Journal of Biological Macromolecules*, *113*, 195–204.
- Zhang, Y., Pan, X., Ran, S., & Wang, K. (2019). Purification, structural elucidation and anti-inflammatory activity in vitro of polysaccharides from *Smilax china* L. *International Journal of Biological Macromolecules*, *139*, 233–243.
- Zhang, Y., Zhou, T., Wang, H., Cui, Z., Cheng, F., & Wang, K. P. (2016). Structural characterization and in vitro antitumor activity of an acidic polysaccharide from *Angelica sinensis* (Oliv.) Diels. *Carbohydrate Polymers*, *147*, 401–408.
- Zhao, G. H., Kan, J. Q., Li, Z. X., & Chen, Z. D. (2005). Structural features and immunological activity of a polysaccharide from *Dioscorea opposita* Thunb roots. *Carbohydrate Polymers*, *61*(2), 125–131.
- Zhao, J., Zhang, F. M., Liu, X. Y., Ange, K. S., Zhang, A. Q., Li, Q. H., & Linhardt, R. J. (2017). Isolation of a lectin binding rhamnagalacturonan-I containing pectic polysaccharide from pumpkin. *Carbohydrate Polymers*, *163*, 330–336.
- Zhu, R., Zhang, X., Wang, Y., Zhang, L., Zhao, J., Chen, G., Fan, J., Jia, Y., Yan, F., & Ning, C. (2019). Characterization of polysaccharide fractions from fruit of *Actinidia arguta* and assessment of their antioxidant and antiglycated activities. *Carbohydrate Polymers*, *210*, 73–84.